J|A|C|S ARTICLES

Published on Web 05/14/2010

Columnar Organization of Head-to-Tail Self-Assembled Pt_4 Rings

Peter D. Frischmann, Samuel Guieu, Raymond Tabeshi, and Mark J. MacLachlan*

Department of Chemistry, University of British Columbia, 2036 Main Mall, Vancouver, British Columbia V6T 1Z1, Canada

Received December 25, 2009; Revised Manuscript Received April 16, 2010; E-mail: mmaclach@chem.ubc.ca

Abstract: Coordination of Pt^{2+} to a family of tunable Schiff base proligands directs the 12-component self-assembly of disk-shaped Pt_4 rings in a head-to-tail fashion. Aggregation of these S_4 symmetric Pt_4 macrocycles into columnar architectures was investigated by dynamic and static light scattering, NMR spectroscopy, powder X-ray diffraction, and transmission electron microscopy. Data from these experiments support the formation of columnar architectures for all of the structures studied except when bulky tris(4-*tert*-butylphenyl)methyl substituents were present. In this case, aggregation was limited to dimers in $CHCl_3$ ($K_{dim} = 3200 \pm 200$ L mol^{-1} at 25 °C) and a thermodynamic analysis revealed that dimerization is an entropy driven process. Columnar architectures of Pt_4 rings with branched 2-hexyldecyl substituents organize into lyotropic mesophases in nonpolar organic solvents. These new self-assembled supramolecules are promising candidates to access nanotubes with multiple linear arrays of Pt^{2+} ions.

Introduction

Self-assembly has emerged as a powerful technique to organize small molecules into functional materials with minimal effort.[1] The morphology of self-assembled materials is dictated by the geometry and chemical functionality of the monomeric constituents.[2] Disk-shaped molecules composed primarily of aromatic units often code for the assembly of one-dimensional fibers or noncovalent nanotubes and are being pursued as materials for photovoltaic active layers, sensors, and molecular wires.[3] Solvophobic and weak intermolecular forces such as hydrogen-bonding or $\pi-\pi$ interactions dominate the self-assembly process of these systems.

Planar coordination complexes also assemble into fibers where anisotropic metal−metal interactions aid in assembly and impart unique properties, often inaccessible with purely organic analogues. Phosphorescent, electrophosphorescent, luminescent, electroluminescent, vapoluminescent, and semiconducting wires have been constructed via self-assembly of neutral or cationic Pt^{2+} complexes coordinated by chelating aromatic ligands.[4] Similar complexes form luminescent metallogels, chromonic liquid crystals, nanosheets, and wheel-shaped superstructures through a subtle balance of Coulombic, metal−metal, and/or $\pi-\pi$ interactions.[5] The exciting properties exhibited by these systems hold promise for development of novel materials.

Platinum−pyridyl chemistry has been extensively investigated in the synthesis of complex molecules. Typically, dipyridyl-based ligands are combined with *cis* or *trans* protected Pt^{2+}

(1) (a) Drain, C. M.; Varotto, A.; Radivojevic, I. *Chem. Rev.* **2009**, *109*, 1630–1658. (b) Lehn, J.-M. *Proc. Natl. Acad. Sci. U.S.A.* **2002**, *99*, 4763–4768. (c) Whitesides, G. M.; Boncheva, M. *Proc. Natl. Acad. Sci. U.S.A.* **2002**, *99*, 4769–4774. (d) Reinhoudt, D. N.; Crego-Calama, M. *Science* **2002**, *295*, 2403–2407.

(2) (a) Hosseini, M. W. *Acc. Chem. Res.* **2005**, *38*, 313–323. (b) Lehn, J.-M. *Science* **2002**, *295*, 2400–2403.

(3) (a) Wong, W. W. H.; Ma, C.-Q.; Pisula, W.; Yan, C.; Feng, X.; Jones, D. J.; Müllen, K.; Janssen, R. A. J.; Bäuerle, P.; Holmes, A. B. *Chem. Mater.* **2010**, *22*, 457–466. (b) Klosterman, J. K.; Yamauchi, Y.; Fujita, M. *Chem. Soc. Rev.* **2009**, *38*, 1714–1725. (c) Yin, M.; Shen, J.; Pisula, W.; Liang, M.; Zhi, L.; Müllen, K. *J. Am. Chem. Soc.* **2009**, *131*, 14618–14619. (d) Reiriz, C.; Brea, R. J.; Arranz, R.; Carrascosa, J. L.; Garibotti, A.; Manning, B.; Valpuesta, J. M.; Eritja, R.; Castedo, L.; Granja, J. R. *J. Am. Chem. Soc.* **2009**, *131*, 11335–11337. (e) Schmaltz, B.; Weil, T.; Müllen, K. *Adv. Mater.* **2009**, *21*, 1067–1078. (f) van Hameren, R.; van Buul, A. M.; Catriciano, M. A.; Villari, V.; Micali, N.; Schön, P.; Speller, S.; Scolaro, L. M.; Rowan, A. E.; Elemans, J. A. A. W.; Nolte, R. J. M. *Nano Lett.* **2008**, *8*, 253–259. (g) Zang, L.; Che, Y.; Moore, J. S. *Acc. Chem. Res.* **2008**, *41*, 1596–1608. (h) Zhao, D.; Moore, J. S. *Chem. Commun.* **2003**, 807–818. (i) Bong, D. T.; Clark, T. D.; Granja, J. R.; Ghadiri, M. R. *Angew. Chem., Int. Ed.* **2001**, *40*, 988–1011.

(4) (a) Kozhevnikov, V. N.; Donnio, B.; Bruce, D. W. *Angew. Chem., Int. Ed.* **2008**, *47*, 6286–6289. (b) Yuen, M.-Y.; Roy, V. A. L.; Lu, W.; Kui, S. C. F.; Tong, G. S. M.; So, M.-H.; Chui, S. S.-Y.; Muccini, M.; Ning, J. Q.; Xu, S. J.; Che, C.-M. *Angew. Chem., Int. Ed.* **2008**, *47*, 9895–9899. (c) Sun, Y.; Ye, K.; Zhang, H.; Zhang, J.; Zhao, L.; Li, B.; Yang, G.; Yang, B.; Wang, Y.; Lai, S.-W.; Che, C.-M. *Angew. Chem., Int. Ed.* **2006**, *45*, 5610–5613. (d) Kui, S. C. F.; Chui, S. S.-Y.; Che, C.-M.; Zhu, N. *J. Am. Chem. Soc.* **2006**, *128*, 8297–8309. (e) Kwok, C.-C.; Ngai, H. M. Y.; Chan, S.-C.; Sham, I. H. T.; Che, C.-M.; Zhu, N. *Inorg. Chem.* **2005**, *44*, 4442–4444. (f) Lu, W.; Mi, B.-X.; Chan, M. C. W.; Hui, Z.; Che, C.-M.; Zhu, N.; Lee, S.-T. *J. Am. Chem. Soc.* **2004**, *126*, 4958–4971. (g) Lin, Y.-Y.; Chan, S.-C.; Chan, M. C. W.; Hou, Y.-J.; Zhu, N.; Che, C.-M.; Liu, Y.; Wang, Y. *Chem.—Eur. J.* **2003**, *9*, 1263–1272.

(5) (a) Tam, A. Y.-Y.; Wong, K. M.-C.; Yam, V. W.-W. *J. Am. Chem. Soc.* **2009**, *131*, 6253–6260. (b) Tam, A. Y.-Y.; Wong, K. M.-C.; Zhu, N.; Wang, G.; Yam, V. W.-W. *Langmuir* **2009**, *25*, 8685–8695. (c) Chen, Y.; Li, K.; Lu, W.; Chui, S. S.-Y.; Ma, C.-W.; Che, C.-M. *Angew. Chem., Int. Ed.* **2009**, *48*, 9909–9913. (d) Lu, W.; Chen, Y.; Roy, V. A. L.; Chui, S. S.-Y.; Che, C.-M. *Angew. Chem., Int. Ed.* **2009**, *48*, 7621–7625. (e) Cardolaccia, T.; Li, Y.; Schanze, K. S. *J. Am. Chem. Soc.* **2008**, *130*, 2535–2545. (f) Lu, W.; Chui, S. S.-Y.; Ng, K.-M.; Che, C.-M. *Angew. Chem., Int. Ed.* **2008**, *47*, 4568–4572. (g) Camerel, F.; Ziessel, R.; Donnio, B.; Bourgogne, C.; Guillon, D.; Schmutz, M.; Iacovita, C.; Bucher, J.-P. *Angew. Chem., Int. Ed.* **2007**, *46*, 2659–2662. (h) Tam, A. Y.-Y.; Wong, K. M.-C.; Wang, G.; Yam, V. W.-W. *Chem. Commun.* **2007**, 2028–2030.

10.1021/ja910886g

Chart 1. Reported N_2O_2 Pt^{2+} Schiff Base Monomer and Conceptual Evolution of the Monomer into a Head-to-Tail Self-Assembling Metallocycle

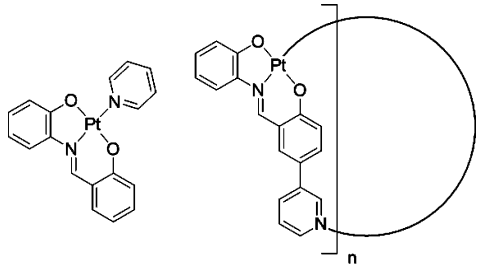

complexes, and highly charged metallocycles are formed.[6] This approach has become a paradigm for development of functional polyhedra, catenanes, and other unique architectures.[7] Despite the variety of interesting structures that have emerged from this method, significant limitations remain. For example, the high charge of the metallocycle has prevented the observation of stacking in solution, a property that could be used to assemble nanotubes that include metal−metal bonding.[8] Also, only high symmetry objects are usually accessible through this method.

Neutral Schiff base platinum(II) complexes with *trans*-N_2O_2 donors, such as the monomer depicted in Chart 1, have been reported,[9] and Bosnich demonstrated that similar complexes are sterically unencumbered for one-dimensional assembly.[10] A solid-state structure revealed close axial Pt···Pt contacts (3.26 Å) between a platinum(II) Schiff base complex and metalated bis(*tert*-pyridyl) pincer hosts, facilitated by $\pi-\pi$ and metallophilic interactions.[11] With the goal of assembling cycles that may ultimately show metal−metal bonding in a columnar orientation, we envisioned a ligand system that codes for the head-to-tail self-assembly of disk-shaped platinum-containing metallocycles as illustrated in Chart 1.

When a single molecule is outfitted with a donor−acceptor pair appropriately distributed to prohibit intramolecular recognition, one end of the molecule recognizes the other end in an intermolecular fashion. The spatial arrangement of this self-recognition determines whether polymers or macrocycles are isolated. Head-to-tail self-assembly facilitated in this fashion has been used to prepare a variety of supramolecules.[12] Through hydrogen bonds and the aid of an alkali metal, G-quartets are a natural example of head-to-tail assembling supramolecules, and synthetic analogues are known to exhibit columnar aggregation.[13]

In this article, we describe a new route to Pt−pyridyl type metallocycles using a head-to-tail synthetic strategy. Self-recognition is achieved by incorporating a coordinating pyridyl ligand and an open (or solvent-occupied) Pt coordination site into the same molecule. Specifically, tetrameric metallocycles are constructed in a selective 12-component, one-pot self-assembly directed by tetradentate Schiff base N−ONO donor proligands formed either *in situ* or prior to metalation. Supramolecular aggregation of individual Pt_4 metallocycles into columnar arrays is observed and bestows liquid crystalline properties upon the materials. These parallel columnar arrays are exciting materials with potential for anisotropic Pt−Pt interactions.

Results and Discussion

We set out to construct the Pt-containing metallocycles shown on the right-hand side of Chart 1. To test the feasibility of this approach and to determine the expected ring size, we first prepared model complex **1**, where the pyridyl group, essential for self-recognition, is substituted by a phenyl group. Single-crystal X-ray diffraction of complex **1**, depicted in Figure 1, shows that the Pt^{2+} is complexed by the ONO Schiff base pocket, and the fourth coordination site is occupied by an S-bound DMSO molecule.[14] Besides the expected rotation of the peripheral phenyl group to relieve steric repulsion between protons (normal for a biphenyl-type system), the molecule is nearly planar. Moreover, the angle of interest for self-assembly, shown in Figure 1a, is approximately 90°, indicating that head-to-tail self-assembly should direct formation of cyclic tetramers if the phenyl group is replaced by a 3-pyridyl unit.

When a solution of model complex **1** in DMSO-d_6 was titrated with pyridine and monitored by ^{1}H NMR spectroscopy, resonances assigned to both free and coordinated pyridine were evident (Figure 2). From integration of these resonances, the equilibrium constant (K_{pyr}) was determined to be 35 ± 14 mol^{-1}

(6) (a) Lee, J.; Ghosh, K.; Stang, P. J. *J. Am. Chem. Soc.* **2009**, *131*, 12028–12029. (b) Northrop, B. H.; Zheng, Y.-R.; Chi, K.-W.; Stang, P. J. *Acc. Chem. Res.* **2009**, *42*, 1554–1563. (c) Northrop, B. H.; Yang, H.-B.; Stang, P. J. *Chem. Commun.* **2008**, 5896–5908. (d) Stang, P. J.; Cao, D. H. *J. Am. Chem. Soc.* **1994**, *116*, 4981–4982.

(7) (a) Yoshizawa, M.; Klosterman, J. K.; Fujita, M. *Angew. Chem., Int. Ed.* **2009**, *48*, 3418–3438. (b) Ghosh, K.; Hu, J.; White, H. S.; Stang, P. J. *J. Am. Chem. Soc.* **2009**, *131*, 6695–6697. (c) Yamashita, K.-I.; Kawano, M.; Fujita, M. *J. Am. Chem. Soc.* **2007**, *129*, 1850–1851. (d) Yoshizawa, M.; Ono, K.; Kumazawa, K.; Kato, T.; Fujita, M. *J. Am. Chem. Soc.* **2005**, *127*, 10800–10801. (e) Sun, S.-S.; Stern, C. L.; Nguyen, S. T.; Hupp, J. T. *J. Am. Chem. Soc.* **2004**, *126*, 6314–6326. (f) Leininger, S.; Olenyuk, B.; Stang, P. J. *Chem. Rev.* **2000**, *100*, 853–908.

(8) For solid-state stacking, see the following: Stang, P. J.; Cao, D. H.; Saito, S.; Arif, A. M. *J. Am. Chem. Soc.* **1995**, *117*, 6273–6283.

(9) Motschi, H.; Nussbaumer, C.; Pregosin, P. S.; Bachechi, F.; Mura, P.; Zambonelli, L. *Helv. Chim. Acta* **1980**, *63*, 2071–2086.

(10) (a) Crowley, J. D.; Steele, I. M.; Bosnich, B. *Inorg. Chem.* **2005**, *44*, 2989–2991. (b) Crowley, J. D.; Steele, I. M.; Bosnich, B. *Eur. J. Inorg. Chem.* **2005**, 3907–3917. (c) Crowley, J. D.; Goshe, A. J.; Bosnich, B. *Chem. Commun.* **2003**, 392–393.

(11) Goshe, A. J.; Steele, I. M.; Bosnich, B. *J. Am. Chem. Soc.* **2003**, *125*, 444–451.

(12) A few examples: (a) Berggren, G.; Thapper, A.; Huang, P.; Kurz, P.; Eriksson, L.; Styring, S.; Anderlund, M. F. *Dalton Trans.* **2009**, 10044–10054. (b) Fernández, G.; Pérez, E. M.; Sánchez, L.; Martín, N. *Angew. Chem., Int. Ed.* **2008**, *47*, 1094–1097. (c) Asadi, A.; Patrick, B. O.; Perrin, D. M. *J. Am. Chem. Soc.* **2008**, *130*, 12860–12861. (d) Jensen, R. A.; Kelley, R. F.; Lee, S. J.; Wasielewski, M. R.; Hupp, J. T.; Tiede, D. M. *Chem. Commun.* **2008**, 1886–1888. (e) Willison, S. A.; Krause, J. A.; Connick, W. B. *Inorg. Chem.* **2008**, *47*, 1258–1260. (f) Zhao, S.-B.; Wang, R.-Y.; Wang, S. *J. Am. Chem. Soc.* **2007**, *129*, 3092–3093. (g) Fernández, J. J.; Fernández, A.; Vázquez-García, D.; López-Torres, M.; Suárez, A.; Gómez-Blanco, N.; Vila, J. M. *Eur. J. Inorg. Chem.* **2007**, 5408–5418. (h) Asadi, A.; Patrick, B. O.; Perrin, D. M. *J. Org. Chem.* **2007**, *72*, 466–475. (i) Brasey, T.; Scopelliti, R.; Severin, K. *Inorg. Chem.* **2005**, *44*, 160–162. (j) Fenniri, H.; Mathivanan, P.; Vidale, K. L.; Sherman, D. M.; Hallenga, K.; Wood, K. V.; Stowell, J. G. *J. Am. Chem. Soc.* **2001**, *123*, 3854–3855. (k) Carina, R. F.; Williams, A. F.; Bernardinelli, G. *Inorg. Chem.* **2001**, *40*, 1826–1832. (l) Matsumoto, N.; Motoda, Y.; Matsuo, T.; Nakashima, T.; Re, N.; Dahan, F.; Tuchagues, J.-P. *Inorg. Chem.* **1999**, *38*, 1165–1173. (m) Stang, P. J.; Whiteford, J. A. *Res. Chem. Intermediat.* **1996**, *22*, 659–665. (n) Kajiwara, T.; Ito, T. *J. Chem. Soc., Chem. Commun.* **1994**, 1773–1774.

(13) (a) Davis, J. T. *Angew. Chem., Int. Ed.* **2004**, *43*, 668–698. (b) Mezzina, E.; Mariani, P.; Itri, R.; Masiero, S.; Pieraccini, S.; Spada, G. P.; Spinozzi, F.; Davis, J. T.; Gottarelli, G. *Chem.—Eur. J.* **2001**, *7*, 388–395.

(14) X-ray crystal data for **1** grown from DMSO: $C_{21}H_{18.5}NO_3PtS$, $M_w = 560.02$ g mol^{-1}, yellow needle, orthorhombic, space group $P2_12_12_1$, $a = 5.5909(5)$ Å, $b = 17.6944(17)$ Å, $c = 19.0577(18)$ Å, $V = 1885.3(3)$ Å^3, $Z = 4$, R1 = 0.0441, wR2 = 0.1146.

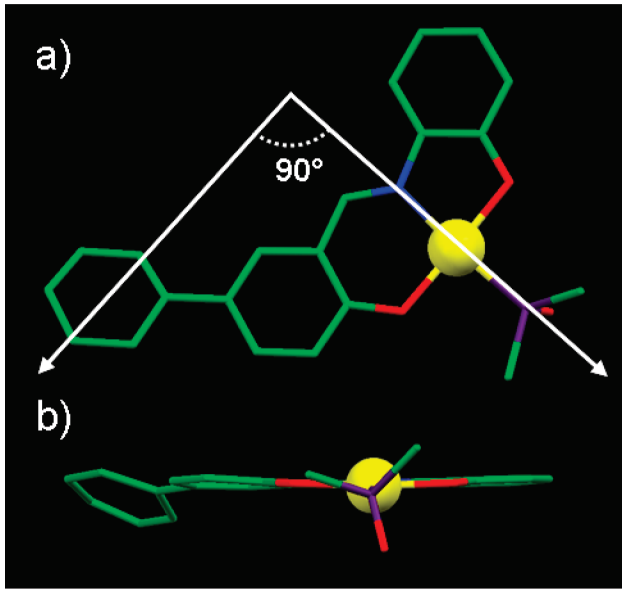

Figure 1. Solid-state structure of complex **1**: (a) top-down view highlighting the 90° angle that directs tetrameric self-assembly when the peripheral phenyl group is replaced by a 3-pyridyl group; b) side-on view. C = green, O = red, N = blue, Pt = yellow, S = purple.

L at 25 °C. This favorable Pt^{2+}−pyridine interaction, even in a competing coordinating solvent, combined with the entropy gain expected upon forming the metallocycle (from displaced solvent) was anticipated to drive the self-assembly of **4a**−**d** as shown in Scheme 1.

In a one-pot experiment where proligand **3a** was generated *in situ*, K_2PtCl_4, K_2CO_3, 5-(3-pyridyl)salicylaldehyde, and *o*-aminophenol were reacted in degassed DMSO at 150 °C for 2 h. Upon cooling of the sample, an air-stable yellow solid precipitated that was isolated by centrifugation and washed with water and MeOH. Solvent free matrix assisted laser desorption ionization time-of-flight mass spectrometry (MALDI-TOF MS) showed the selective formation of the cyclic tetramer, **4a** (m/z = 1934), with no other oligomers or ring sizes observed. Most interestingly, the only higher mass peaks observed correspond to sequential aggregates from dimer, $[\mathbf{4a}_2]^+$, up to hexamer, $[\mathbf{4a}_6]^+$, due to columnar aggregation, as shown in Figure 3.

As Pt_4 ring **4a** is insoluble in all common solvents, we pursued 2-hexyldecyl substituted Pt_4 ring **4b** as a soluble alternative in order to perform solution NMR spectroscopic studies. Although **4a**−**d** may all be prepared *in situ* from the imine precursors (i.e., the aldehyde and aminophenol), starting from proligands **3a**−**d** gives better results. In this manner, cyclic tetramer **4b** was selectively synthesized (Scheme 1) and its identity confirmed by MALDI-TOF MS. Aggregation of Pt_4 rings was again evident, with a series of peaks observed up to m/z = 14 168, corresponding to $[\mathbf{4b}_5]^+$. ^{1}H NMR spectroscopy of **4b** in $CDCl_3$, C_6D_6, and toluene-d_8 produced only broad unidentifiable resonances even at elevated temperatures. This broadening is attributed to a substantial decrease in the T_2 relaxation time,[15] providing further evidence for strong interactions between Pt_4 rings resulting in polymeric aggregation. Clearly bulkier substituents are necessary to inhibit stacking for an NMR spectroscopic study.

Pt_4 ring **4c** with bulky trityl substituents was synthesized (Scheme 1). Unfortunately, **4c** is also poorly soluble. MALDI-TOF MS analysis, however, revealed formation of not only cyclic tetramer **4c** but also aggregates up to $[\mathbf{4c}_6]^+$. We prepared proligand **3d** with even bulkier tris(4-*tert*-butylphenyl)methyl substituents and used this compound to synthesize Pt_4 ring **4d**. Despite observing aggregates up to $[\mathbf{4d}_5]^+$ in the MALDI-TOF MS, **4d** is very soluble in organic solvents. Metallocycles **4b**−**d** are all brightly colored yellow solids that show absorption bands around 300−310, 425−430, and 450−455 nm (see Supporting Information Figure S9 for spectra).

The ^{1}H NMR spectrum of **4d** in $CDCl_3$ (see Figure 4a) exhibits sharp resonances that were assigned by COSY and ROESY 2D NMR spectroscopy.[16] The low intensity resonances in the spectrum that appear to be impurities exhibit strong cross peaks with the identified resonances in the ROESY spectrum, indicative of chemical exchange. A variable concentration ^{1}H NMR spectroscopic experiment revealed that the identified resonances are in fact due to an aggregate and the low intensity resonances are assigned to monomers. Equilibrium constants calculated by integration of ^{1}H NMR spectra collected between −45 and 25 °C fit best to a monomer−dimer rather than infinite aggregate model,[17] as might be expected for such sharp resonances (Figure 4b). At 25 °C, $K_{dim} = 3200 \pm 200$ L mol^{-1} and a van't Hoff analysis (Figure 4c) gave $\Delta H° = 13 \pm 1$ kJ mol^{-1} and $\Delta S° = 110 \pm 30$ J mol^{-1} K^{-1}. This result indicates that dimerization is enthalpy opposed but entropy favored. The entropy increase in this process is attributed to the release of solvating $CDCl_3$ molecules upon dimerization.[18] Extended aggregation of **4d** in the solid state, as observed by MALDI-TOF MS, is inhibited in solution by rapid rotation of the tris(4-^{t}BuPh) substituents. As very bulky substituents are necessary to limit the aggregation even to dimers, as in the case of **4d**, we conclude that macrocycle **4b** with much smaller substituents aggregates extensively in solution, explaining its broad ^{1}H NMR spectrum.

Because we have been unable to obtain single crystals of **4a**−**d**, we undertook an *ab initio* DFT study of complex **4a** to learn more about its structure and as a model for aggregation. Figure 5a shows the puckered conformation of **4a** determined by DFT optimization.[19] This conformation exhibits a 60° deviation from planarity, a maximum outer diameter of 2.4 nm, and a 0.7 nm inner pore. The intermetallic Pt−Pt distances in the macrocycle are 1.5 nm (diagonal) and 1.1 nm (edge). Belonging to the rare point group S_4, this geometry is imposed by the 38° dihedral angle between the 3-pyridyl and phenyl rings of the salicylidene unit.[20]

Modeling studies reveal that the puckered Pt_4 rings may organize into columns either with a single orientation (*syn*) or

(15) Evertsson, H.; Nilsson, S.; Welch, C. J.; Sundelöf, L.-O. *Langmuir* **1998**, *14*, 6403–6408.

(16) The ^{1}H NMR spectrum of **4d** in CD_2Cl_2 is significantly complicated relative to the spectrum obtained in $CDCl_3$ because of either adoption of a lower symmetry conformation or oligomeric aggregation being facilitated by CD_2Cl_2 (see Supporting Information Figure S5 for spectra).

(17) Martin, R. B. *Chem. Rev.* **1996**, *96*, 3043–3064.

(18) Entropy-driven dimerization: (a) Frischmann, P. D.; Facey, G. A.; Ghi, P. Y.; Gallant, A. J.; Bryce, D. L.; Lelj, F.; MacLachlan, M. J. *J. Am. Chem. Soc.* **2010**, *132*, 3893–3908. (b) Kang, J.; Rebek, J., Jr. *Nature* **1996**, *382*, 239–241. (c) Cram, D. J.; Choi, H. J.; Bryant, J. A.; Knobler, C. B. *J. Am. Chem. Soc.* **1992**, *114*, 7748–7765. (d) Frischmann, P. D.; MacLachlan, M. J. *Chem. Commun.* **2007**, 4480–4482.

(19) Optimization with B3LYP level of theory (LanL2dZ basis sets for Pt, 6-31G* for other atoms): Yamashita, K.; Sato, K.; Kawano, M.; Fujita, M. *New J. Chem.* **2009**, *33*, 264–270.

(20) Other supramolecules with S_4 symmetry: (a) Su, C.-Y.; Smith, M. D.; zur Loye, H.-C. *Angew. Chem., Int. Ed.* **2003**, *42*, 4085–4089. (b) Beissel, T.; Powers, R. E.; Raymond, K. N. *Angew. Chem., Int. Ed.* **1996**, *33*, 1084–1086.

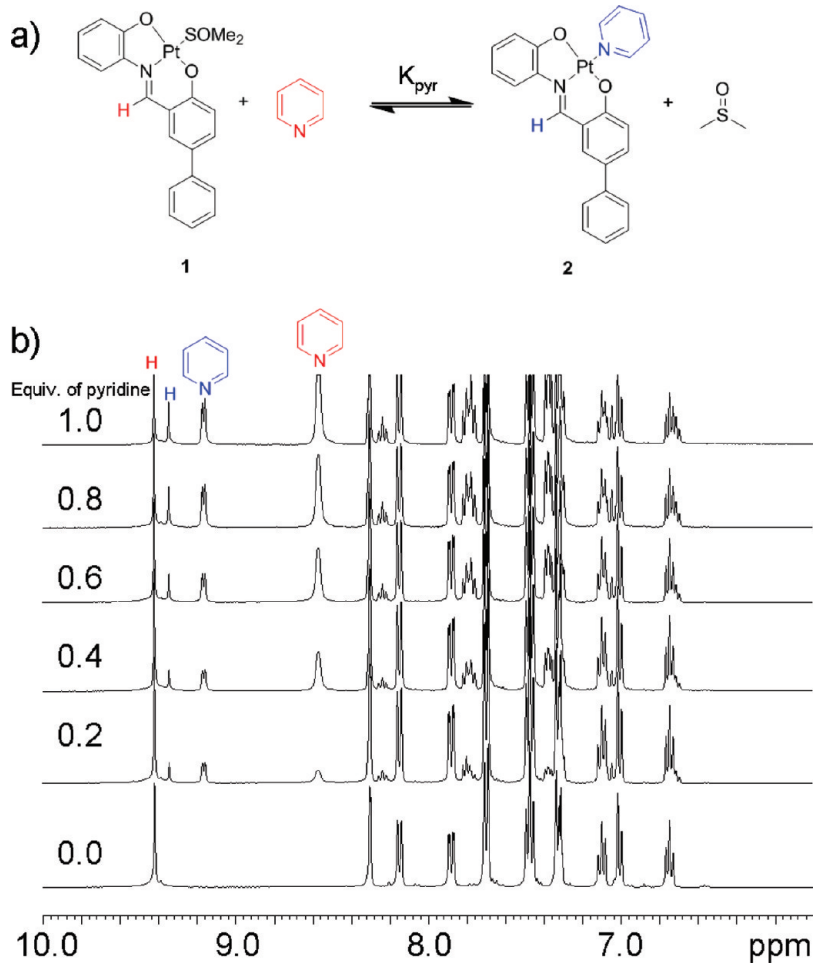

Figure 2. (a) Equilibrium between DMSO-bound model complex **1** and pyridine-bound model complex **2**. (b) ^{1}H NMR spectra of model complex **1** in DMSO-d_6 when titrated with pyridine (25 mmol L^{-1}, 400 MHz). Equivalents of pyridine are given on the left, and the resonances integrated for thermodynamic analysis are color-coded on top.

Scheme 1. Head-to-Tail Self-Assembly of Pt_4 Rings **4a**−**d**[a]

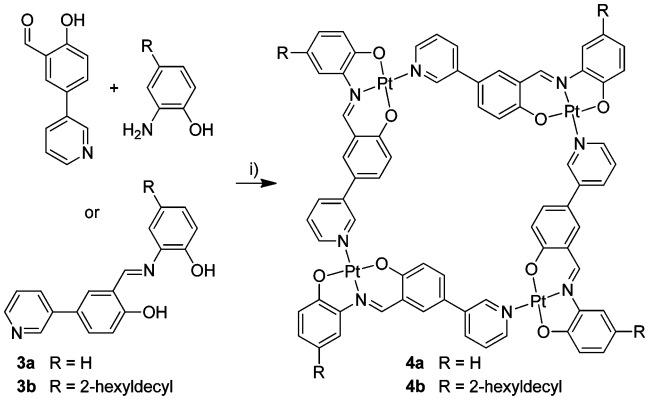

[a] (i) N−ONO salicylaldimine proligand **3a**−**d** (or corresponding amine and aldehyde), K_2CO_3, and K_2PtCl_4 are heated in DMSO at 150 °C for 2−4 h.

with alternating orientations (*anti*), depending on the steric bulk of the peripheral R group (Figure 5b). In the *syn* case, the repeat unit is a simple translation along the columnar axis, whereas the *anti* orientation requires the same translation, a 90° rotation about the columnar axis and a 180° rotation perpendicular to the columnar axis. With small substituents, the cycles may adopt

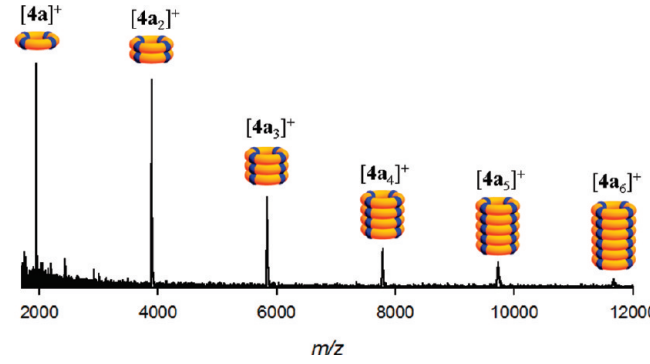

Figure 3. Aggregates of Pt_4 ring **4a** observed with MALDI-TOF MS.

either stacking motif, but with sterically demanding substituents, only the *anti* alternating, AB pattern is possible because this reduces intermolecular interactions between the substituents. Potential for intermolecular Pt−Pt interaction exists in the *syn* case.

Solution aggregation of Pt_4 rings **4b** and **4d** in $CHCl_3$ was further investigated by dynamic and multiangle laser light scattering (DLS and MALLS, respectively). The ^{1}H NMR studies of **4d** described above indicated that aggregation in solution was limited to dimers. DLS of **4d** (0.6 mg mL^{-1}) showed that only aggregates of <10 nm in diameter are present, confirming that dimerization and not infinite aggregation is occurring. On the other hand, DLS of **4b** (0.6 mg mL^{-1}) resulted

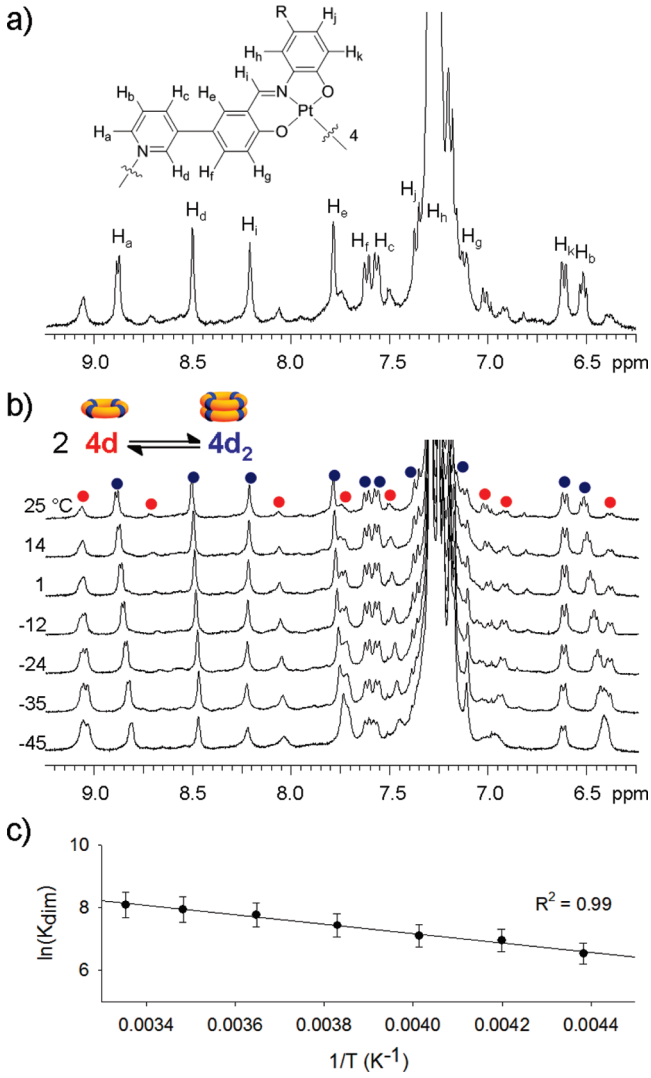

Figure 4. (a) ^{1}H NMR spectrum of **4d** in $CDCl_3$ (400 MHz) and an inset of the chemical structure. Resonances of the peripheral, R = tris(4-^{t}BuPh), aromatic rings overlap with the residual $CHCl_3$ resonance calibrated to 7.27 ppm. (b) Variable temperature ^{1}H NMR spectra of **4d** in $CDCl_3$ (2 mmol L^{-1}) from −45 to 25 °C. Monomer−dimer equilibrium is shown, and resonances are color-coded (monomer = red, dimer = blue). (c) van't Hoff plot for dimerization of **4d** in $CDCl_3$.

in a broad peak corresponding to a hydrodynamic radius (R_H) of 60 nm (assuming spherical particles).[21]

To obtain information about the shape of the aggregates of **4b** in solution, a MALLS study was undertaken. Columnar aggregation of **4b** was confirmed by the Kratky plot, shown in Figure 6a, that exhibits linear angular dependence over the light scattering intensity of the aggregates.[22] A Zimm plot was also constructed from MALLS data over a 0.4−0.8 mg mL^{-1}

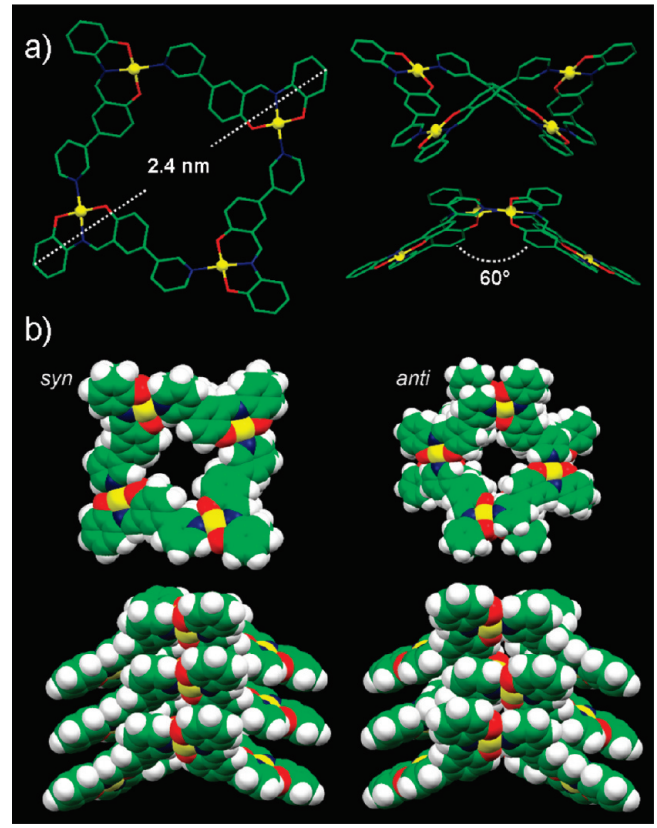

Figure 5. (a) DFT optimized geometry of Pt_4 ring **4a**. (b) Computer model of two possible orientations for columnar aggregation. Each ring is stacked directly on the other in the *syn* orientation, whereas the *anti* orientation exhibits alternating AB type stacking.

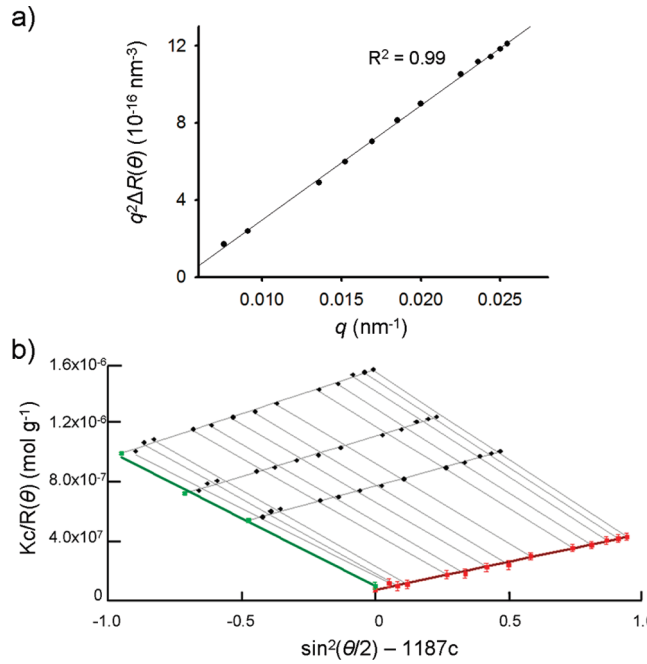

Figure 6. MALLS analysis of **4b** in $CHCl_3$: (a) Kratky plot (0.6 mg mL^{-1}); (b) Zimm plot (0.4, 0.6, and 0.8 mg mL^{-1}).

concentration range and is shown in Figure 6b with extrapolations to zero concentration and angle. From the Zimm analysis we obtained an average molecular weight, $M_w = (1.2 \pm 0.4) \times 10^7$ g mol^{-1}, radius of gyration, $R_g = 150 \pm 17$, and a second

(21) Goldin, A. A. DYNALS, version 2.0. Software for particle size distribution analysis in photon correlation spectroscopy. http://www.softscientific.com/science/WhitePapers/dynals1/dynals100.htm (accessed April 13, 2010).

(22) (a) Ryu, J.-H.; Tang, L.; Lee, E.; Kim, H.-J.; Lee, M. *Chem.—Eur. J.* **2008**, *14*, 871–881. (b) Ryu, J.-H.; Lee, E.; Lim, Y.-B.; Lee, M. *J. Am. Chem. Soc.* **2007**, *129*, 4808–4814. (c) Yang, W.-Y.; Lee, E.; Lee, M. *J. Am. Chem. Soc.* **2006**, *128*, 3484–3485. (d) Kim, B.-S.; Hong, D.-J.; Bae, J.; Lee, M. *J. Am. Chem. Soc.* **2005**, *127*, 16333–16337. (e) Rosselli, S.; Ramminger, A.-D.; Wagner, T.; Silier, B.; Wiegand, S.; Häussler, W.; Lieser, G.; Scheumann, V.; Höger, S. *Angew. Chem., Int. Ed.* **2001**, *40*, 3137–3141. (f) Bockstaller, M.; Köhler, W.; Wegner, G.; Vlassopoulos, D.; Fytas, G. *Macromolecules* **2000**, *33*, 3951–3953.

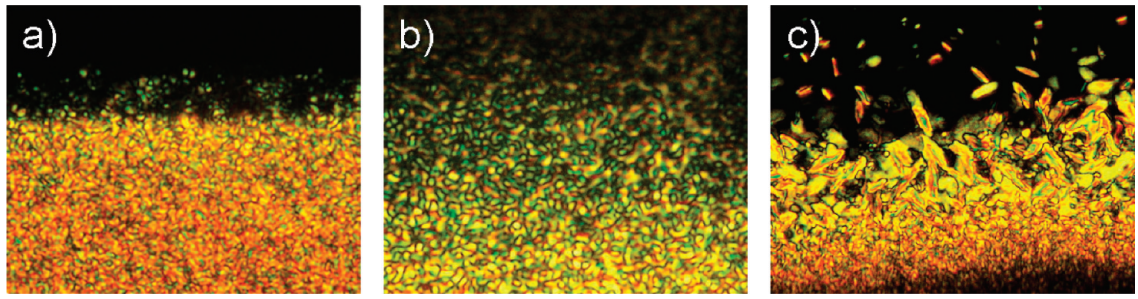

Figure 7. POM images observed under crossed polarizers of growing LC textures for **4b** from (a) $CHCl_3$ and (b, c) PhCl. Black indicates an isotropic phase.

virial coefficient, $A_2 = (5.4 \pm 0.4) \times 10^{-4}$ mol mL g^{-2}. Although the aggregates in this system are dynamic in nature (owing to noncovalent interactions), making these values nonquantitative, they are still reasonably reliable for making predictions about the system.[23] In particular, spherical or random coil aggregates exhibit R_g/R_H ratios below 1.5 whereas for rigid rod-shaped aggregates the ratio is greater.[24] The R_g/R_H ratio for Pt_4 ring **4b** is 2.5, indicating these are highly anisotropic rigid column/rod-shaped aggregates. Attempts to elucidate the thermodynamics of columnar aggregation in $CHCl_3$ by variable concentration UV−vis experiments were inhibited because there is no change in the absorption spectra from 3.4×10^{-4} to 2.6×10^{-6} mol L^{-1}, suggesting that even at very low concentrations **4b** is extensively aggregated.

We were surprised to discover that columnar aggregates of Pt_4 ring **4b** organize into lyotropic mesophases upon concentration in nonpolar organic solvents. Liquid crystalline (LC) behavior was observed in $CHCl_3$, C_6H_6, PhCl, trichloroethylene, CS_2, and pyridine; however, the highest quality mesophases, as judged by the homogeneity of the texture, are obtained in chlorobenzene.[25] Birefringence of these LCs was observed with a polarized optical microscope (POM) upon slow evaporation of dropcast solutions on a microscope slide, and typical POM images of **4b** are depicted in Figure 7.[26] The steric bulk of Pt_4 rings **4c** and **4d** inhibits extended columnar aggregation, and accordingly little to no birefringence is observed for these metallocycles in the same solvents.

Most often, threadlike or Schlieren textures are observed for **4b**, suggesting the adoption of a columnar nematic LC phase.[27] In Figure 7c, a fan-shaped texture is observed near the isotropic phase, potentially due to adoption of a disordered hexagonal columnar mesophase.[28] The S_4 symmetry of **4b** may inhibit organization of a high fidelity hexagonal columnar LC phase leading to a more disordered phase. In all cases, the anisotropy of rod-shaped aggregates self-assembled from **4b** leads to long-range parallel orientation of columns in concentrated solutions and adoption of nematic and/or disordered hexagonal columnar LC phases as outlined in Scheme 2.[29] This is the first report of lyotropic liquid crystallinity for Pt−pyridyl metallocycles and a rare example of a multimetallic LC.[30]

Organization of the Pt_4 rings was also studied in the solid state by powder X-ray diffraction (PXRD). Figure 8a−d shows the PXRD patterns of microcrystalline **4a**−**d** immediately after isolation. Unsubstituted Pt_4 ring **4a** displays the most crystallinity, with several sharp peaks present in the powder pattern. Unfortunately, there are too few peaks to obtain a space group or even a definitive unit cell, but the best fits to the experimental data were for tetragonal unit cells ($\alpha = \beta = \gamma = 90°$) with $a = b = 2.043$ or 2.890 nm and $c = 0.5-0.7$ nm.[31,32] This pattern certainly does not prove a columnar stacking of the macrocycles, but the data are consistent with such an arrangement. If the cycles of **4a** were stacked one on top of another as shown in Figure 5 into parallel columns, the intercolumn center-to-center distance would be about 2.1 nm and the intermacrocycle separation in the columns would be around 0.5 nm.

Low-angle peaks are observed at 3.1, 2.9, and 3.2 nm for **4b**, **4c**, and **4d**, respectively. These roughly correspond to the expected intercolumnar distance for parallel aligned aggregates, allowing for interdigitation of the peripheral substituents. Additional low-intensity peaks at higher angle support the presence of some order within each column.

We were unable to directly identify the phases of the lyotropic LCs from PXRD patterns collected of samples in capillary tubes.

(23) Lortie, F.; Boileau, S.; Bouteiller, L.; Chassenieux, C.; Lauprêtre, F. *Macromolecules* **2005**, *38*, 5283–5287.
(24) (a) Runge, M. B.; Dutta, S.; Bowden, N. B. *Macromolecules* **2006**, *39*, 498–508. (b) Schärtl, W. *Light Scattering from Polymer Solutions and Nanoparticle Dispersions*; Springer-Verlag: Berlin and Heidelberg, Germany, 2007.
(25) Because of low solubility of **4b** in cyclohexanone, only small LC domains were observed in this solvent prior to drying.
(26) The critical concentration for birefringence is difficult to estimate, as it is observed only upon evaporation. In each example the concentration is >1 mg mL^{-1}.
(27) Dierking, I. *Textures of Liquid Crystals*; Wiley-VCH Verlag: Weinheim, Germany, 2003.
(28) Saez, I. M.; Goodby, J. W.; Richardson, R. M. *Chem.—Eur. J.* **2001**, *7*, 2758–2764.
(29) For reviews on columnar LCs, see the following: (a) Kato, T.; Yasuda, T.; Kamikawa, Y.; Yoshio, M. *Chem. Commun.* **2009**, 729–739. (b) Laschat, S.; Baro, A.; Steinke, N.; Giesselmann, F.; Hägele, C.; Scalia, G.; Judele, R.; Kapatsina, E.; Sauer, S.; Schreivogel, A.; Tosoni, M. *Angew. Chem., Int. Ed.* **2007**, *46*, 4832–4887.
(30) (a) Cordovilla, C.; Coco, S.; Espinet, P.; Donnio, B. *J. Am. Chem. Soc.* **2010**, *132*, 1424–1431. (b) Coco, S.; Cordovilla, C.; Donnio, B.; Espinet, P.; García-Casas, M. J.; Guillon, D. *Chem.—Eur. J.* **2008**, *14*, 3544–3552. (c) Domracheva, N.; Mirea, A.; Schwoerer, M.; Torre-Lorente, L.; Lattermann, G. *ChemPhysChem* **2006**, *7*, 2567–2577. (d) Binnemans, K.; Lodewyckx, K.; Cardinaels, T.; Parac-Vogt, T. N.; Bourgogne, C.; Guillon, D.; Donnio, B. *Eur. J. Inorg. Chem.* **2006**, 150–157. (e) Bilgin-Eran, B.; Tschierske, C.; Diele, S.; Baumeister, U. *J. Mater. Chem.* **2006**, *16*, 1136–1144. (f) Binnemans, K.; Lodewyckx, K.; Donnio, B.; Guillon, D. *Chem.—Eur. J.* **2002**, *8*, 1101–1105. (g) Nesrullajev, A.; Bilgin-Eran, B.; Kazanci, N. *Mater. Chem. Phys.* **2002**, *76*, 7–14. (h) Nesrullajev, A.; Bilgin-Eran, B.; Singer, D.; Kazanci, N.; Praefcke, K. *Mater. Res. Bull.* **2002**, *37*, 2467–2482. (i) Donnio, B. *Curr. Opin. Colloid Interface Sci.* **2002**, *7*, 371–394.
(31) Shirley, R. *Crysfire. An Interactive Powder Indexing Support System*; The Lattice Press: Surrey, U.K., 2004.
(32) The distinct peaks observed at low angle in the diffraction pattern fit best to a tetragonal unit cell. The lack of well-defined peaks beyond ~19° 2θ, which give information about the third parameter (c), makes it very difficult to obtain any reliable measure of c. For unit cells found with $a = b = 2.043$ nm, the best value of c was either 0.44 or 0.49 nm. For the unit cells found with $a = b = 2.890$ nm, the value of c was in the 0.57−0.68 nm range.

Scheme 2. Dynamic Assembly of Pt_4 Ring **4b** into Randomly Oriented Oligomers, Elongated and Oriented Columns, and Columnar Nematic or Disordered Hexagonal Columnar Mesophases upon Concentration

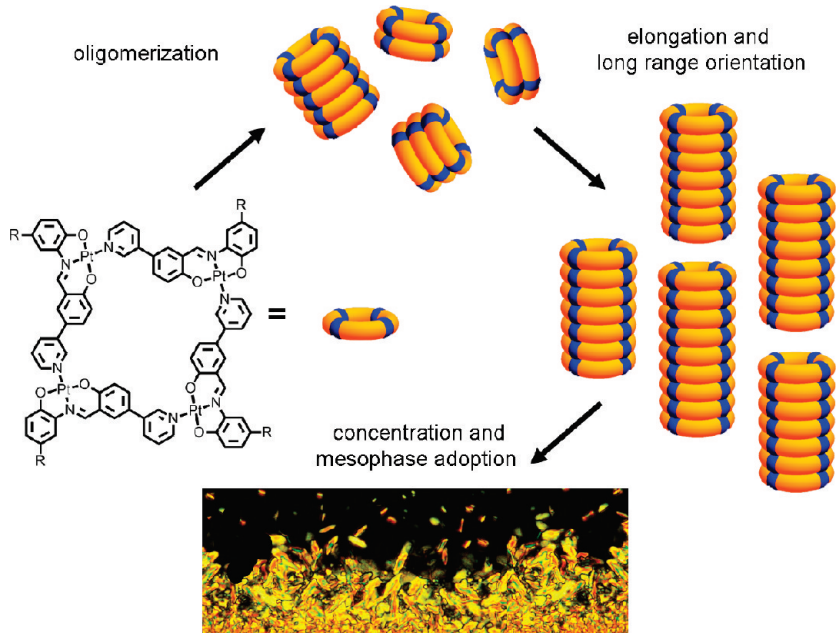

Instead, we collected PXRD data from samples of **4b** in $CHCl_3$ and PhCl that were dropcast onto amorphous silicon plates and left to dry. Diffractograms of the dried LC phases are shown in Figure 8e,f.[33] The low-angle diffraction observed for the sample obtained from $CHCl_3$ (with a peak at 3.1 nm) is nearly identical to that observed in the PXRD pattern of as-isolated **4b**, suggesting that columnar alignment of the nematic phase is being maintained upon drying. Disorder is evident from broad peaks centered about 1.6 and 1.1 nm, preventing any further structural elucidation. PXRD of **4b** dropcast from PhCl shows significantly more order, and a sharp peak is present at 3.5 nm. Close inspection of the low-angle region reveals a broad peak centered about 3.1 nm (10) followed by relatively sharp peaks at 1.8 (11), 1.5 (20), and 1.2 nm (21), diagnostic spacing for hexagonal columnar ordering. These observations are in agreement with POM images that show **4b** adopts both columnar nematic and hexagonal columnar mesophases in PhCl. Intercolumnar spacing is greater for the less ordered columnar nematic phase (3.5 vs 3.1 nm). Overall, the PXRD studies of the films dried from the lyotropic LC phases support the retention of columnar organization in the metallocycles.

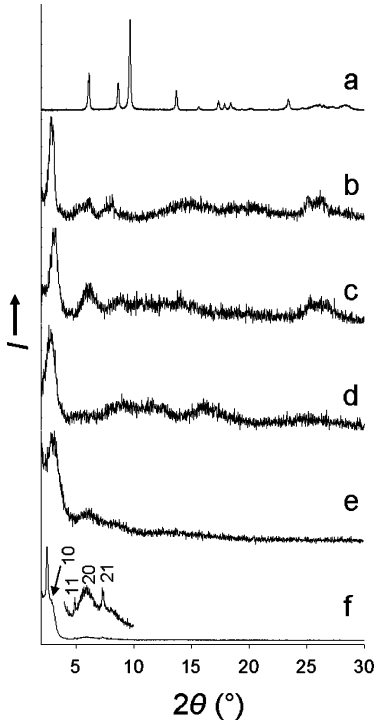

Figure 8. Normalized wide-angle PXRD patterns of as-prepared Pt_4 rings: (a) **4a**, (b) **4b**, (c) **4c**, (d) **4d**, (e) dried mesophase of **4b** drop-cast from $CHCl_3$ onto amorphous silicon, and (f) dried mesophase of **4b** dropcast from PhCl onto amorphous silicon with assigned indices for hexagonal ordering. All data are depicted from 2° to 30° 2θ.

Solid-state organization of Pt_4 ring **4b** was also investigated by transmission electron microscopy (TEM); representative micrographs are shown in Figure 9. At low magnification, we observe oblong "pill-shaped" aggregates assembled from cyclohexanone. High magnification of the same sample reveals each "pill" is composed of individual stacks of Pt_4 rings organized into parallel columnar arrays, as shown in Figure 10. The parallel columns are spaced by roughly 4 nm and extend hundreds of nanometers. When **4b** was deposited on the TEM grid from $CHCl_3$, bundles of randomly oriented rigid rods with dimensions from tens to hundreds of nanometers were observed. This is in agreement with the MALLS data that confirmed the existence of rigid-rod shaped aggregates of **4b** in $CHCl_3$. Micrographs of **4b** deposited from C_6H_6 depict large flexible fibers that are hundreds of nanometers in diameter and span micrometers. The breadth of the rods and fibers observed for **4b** cast from $CHCl_3$ and C_6H_6 suggests that they are also composed of individual columnar arrays, similar to those observed from cyclohexanone; however, we were unable to achieve a similar image resolution in these cases. Organization of individual Pt_4 rings to micrometer length fibers represents an impressive hierarchical self-assembly that spans several orders of magnitude in length, all in one pot. Only diffuse,

(33) Because of the low solubility of **4b** in cyclohexanone, dropcast films were insufficiently thick for PXRD analysis.

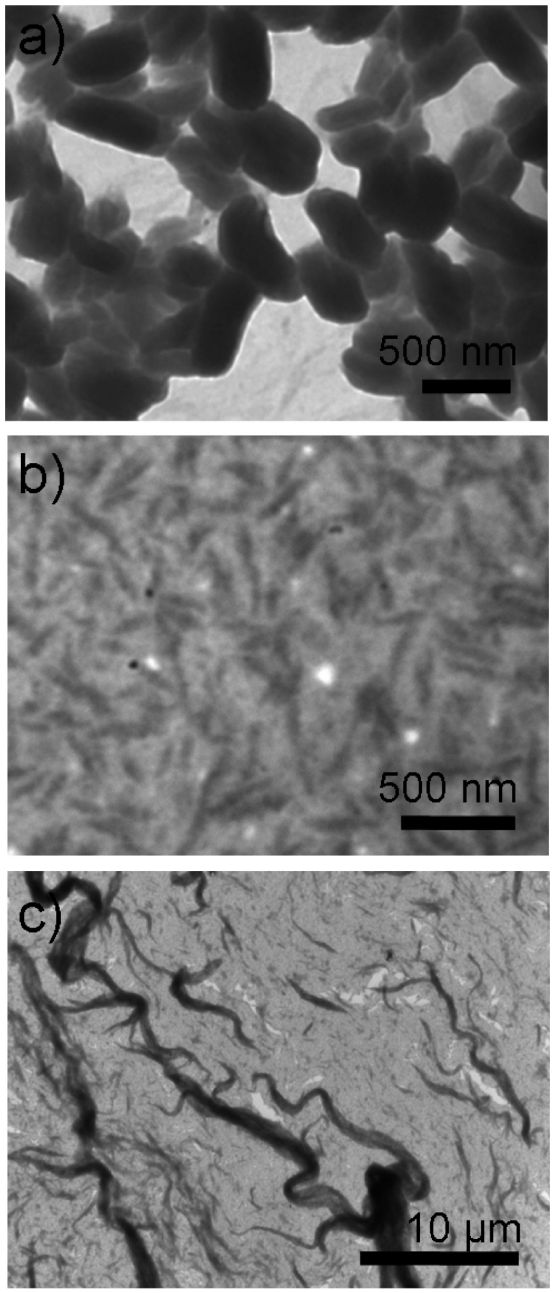

Figure 9. Low magnification TEM images of Pt_4 ring **4b** dried from various solvents: (a) "pill-shaped" oblate aggregates from cyclohexanone; (b) rigid rod-shaped bundles from $CHCl_3$; (c) micrometer length flexible fibers from C_6H_6.

globular aggregates were present in TEM images of sterically encumbered Pt_4 ring **4d**.

Conclusions

We have developed a new class of highly tunable proligands that selectively self-assemble into novel S_4 symmetric disk-shaped metallocycles upon platinum(II) coordination. This head-to-tail approach offers a very flexible, simple method to develop Pt-containing macrocycles en route to nanotubes. Data from light scattering, X-ray diffraction, and transmission electron microscopy support the formation of 1D columnar aggregates from the rings. Although some molecular squares formed with

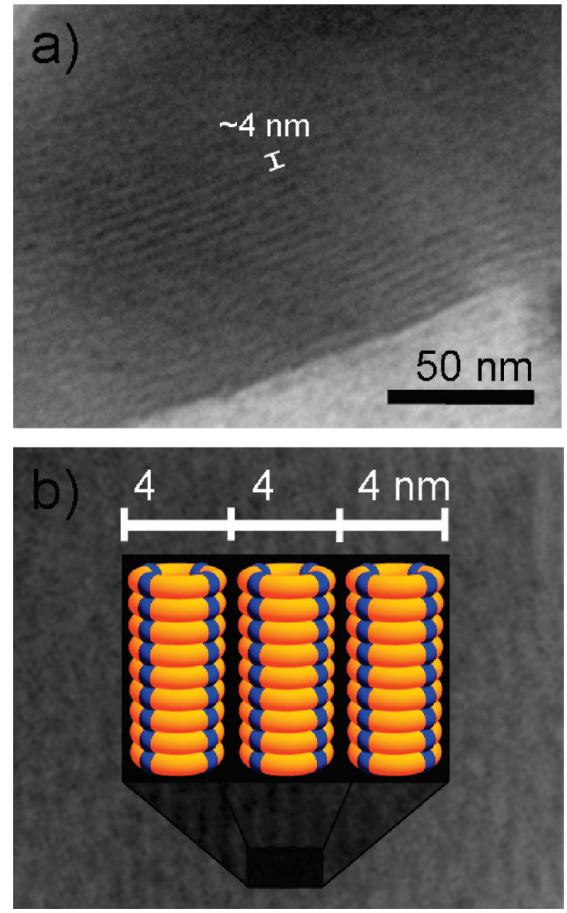

Figure 10. High magnification TEM images of Pt_4 ring **4b** from cyclohexanone: (a) individual columnar arrays visible with periodic spacing of roughly 4 nm; (b) model of columnar aggregates.

Pt−pyridyl bonding exhibit columnar organization in the solid state, to the best of our knowledge no reports of solution aggregation exist, a fact we attribute to Coulombic repulsion. Neutral Pt_4 rings presented here stack strongly both in the solid state and in solution, where they form lyotropic LCs when concentrated. By changing the substituents and the orientation of the *N*-pyridyl group, we expect that diverse metallocycles and self-assembled architectures may be prepared. We are investigating the supramolecular chemistry of these Pt_4 rings to construct conductive nanotubes and liquid crystalline materials.

Acknowledgment. We thank the Natural Sciences and Engineering Research Council (NSERC) of Canada for funding (Discovery grant), UBC for a graduate fellowship (to P.D.F.), Johan Janzen for assistance with the light scattering experiments and analysis, Joseph Hui for TEM images, and Angela Crane for DFT calculations performed with resources provided by Westgrid & Compute/Calcul Canada. S.G. thanks the French Ministry of Foreign and European Affairs for a Lavoisier Postdoctoral Fellowship.

Supporting Information Available: Crystallographic information in CIF format and details of syntheses, characterization, structure coordinates, and calculations. This material is available free of charge via the Internet at http://pubs.acs.org.

JA910886G